AGU ADVANCING EARTH AND SPACE SCIENCES

AGU Advances

RESEARCH ARTICLE
10.1029/2024AV001206

Water Vapor Spectroscopy and Thermodynamics Constrain Earth's Tropopause Temperature

Brett A. McKim[1,2], **Nadir Jeevanjee**[3], **Geoffrey K. Vallis**[2], **and Neil T. Lewis**[2]

[1]Now at LMD/IPSL, Sorbonne Université, CNRS, Paris, France, [2]Department of Mathematics and Statistics, University of Exeter, Exeter, UK, [3]Geophysical Fluid Dynamics Laboratory, Princeton, NJ, USA

Peer Review The peer review history for this article is available as a PDF in the Supporting Information.

Key Points:

- We propose a constraint on Earth's radiative tropopause temperature, stemming from water vapor spectroscopy and thermodynamics
- The predictions of this constraint are borne out quantitatively in both single column and general circulation model experiments
- Our derivation and results confirm and support a Fixed Tropopause Temperature hypothesis

Supporting Information:

Supporting Information may be found in the online version of this article.

Correspondence to:

B. A. McKim,
brettmckim@gmail.com

Citation:

McKim, B. A., Jeevanjee, N., Vallis, G. K., & Lewis, N. T. (2025). Water vapor spectroscopy and thermodynamics constrain Earth's tropopause temperature. *AGU Advances*, *6*, e2024AV001206. https://doi.org/10.1029/2024AV001206

Received 6 FEB 2024
Accepted 14 MAR 2025

Author Contributions:

Conceptualization: Brett A. McKim, Nadir Jeevanjee, Geoffrey K. Vallis
Data curation: Brett A. McKim
Formal analysis: Brett A. McKim
Investigation: Brett A. McKim, Nadir Jeevanjee, Geoffrey K. Vallis
Methodology: Brett A. McKim, Nadir Jeevanjee, Geoffrey K. Vallis, Neil T. Lewis
Project administration: Brett A. McKim
Software: Brett A. McKim, Neil T. Lewis
Supervision: Nadir Jeevanjee, Geoffrey K. Vallis
Validation: Brett A. McKim
Visualization: Brett A. McKim

Abstract As Earth warms, the tropopause is expected to rise, but predictions of its temperature change are less certain. Longstanding theories employing "gray" radiation tie the tropopause temperature to outgoing longwave radiation (OLR), but this is in contrast to recent work in which simulations exhibit a Fixed Tropopause Temperature (FiTT) even as OLR increases. The FiTT is thought to result from the interaction between upper tropospheric moisture and radiation, but a predictive theory for FiTT has not yet been formulated. Here, we build on a recent explanation for the temperature of anvil clouds and argue that tropopause temperature, defined by where radiative cooling becomes negligible, is set by water vapor's maximum spectroscopic absorption and Clausius-Clapeyron scaling. This "thermospectric constraint" makes quantitative predictions for tropopause temperature that are borne out in single column and general circulation model experiments where the spectroscopy is modified and both the radiative and lapse-rate tropopause change in response. This constraint provides a theoretical foundation for the FiTT hypothesis and a more refined explanation for why the tropopause rises with surface warming, shows how tropopause temperature can decouple from OLR, suggests a way to relate the temperatures of anvil clouds and the tropopause, and shows how spectroscopy manifests in Earth's general circulation.

Plain Language Summary The tropopause is the boundary between the troposphere and the stratosphere, but theories disagree on the mechanisms that determine its temperature. It has been argued that the tropopause occurs where water vapor becomes so sparse that it can no longer emit radiation to space. Here we argue that the temperature at which this occurs is set by how sensitive water vapor is to temperature, and how effective it is in blocking and emitting radiation. Our theory leads to precise predictions of tropopause temperature and its small change with surface warming. We verify our theory's mechanism by varying the effectiveness of water vapor absorption in climate models and find the tropopause temperature to change consistently with our theory's predictions. Our results suggest a role for wavelength-dependent radiation physics in constraining the large scale motions of Earth's atmosphere and their change with global warming.

1. Introduction

The tropopause separates the strong surface-driven overturning troposphere from a more gently overturning stratosphere. Understanding the mechanisms setting tropopause temperature and height remains a fundamental and important unsolved problem in climate science (Phillips, 1956)—fundamental because it depends on how two branches of climate, dynamics and radiation, interact (Schneider, 2008; Vallis, 2017); important because the tropopause is a boundary condition in hurricane intensity (Emanuel, 2006; Emanuel et al., 2013), convectively available potential energy (Romps, 2016), CO_2 forcing (Jeevanjee et al., 2021), the water vapor feedback (Feng et al., 2023; Koll et al., 2023; Meraner et al., 2013), stratospheric water vapor (Mote et al., 1996), and ozone destruction (Match & Gerber, 2022).

The dynamically active troposphere exhibits a balance between net radiative cooling and heating from convection and eddies, whereas the stratosphere is closer to radiative equilibrium (zero net radiative heating or cooling). This has led some authors to employ a radiative definition of the tropopause as the lowest level at which the atmosphere attains radiative equilibrium, often in idealized or textbook contexts (Held, 1982; Pierrehumbert, 2010; Thuburn & Craig, 2000; Vallis, 2017) but also in more realistic settings (Gettelman et al., 2004; Lin et al., 2017). We focus on this radiative definition, but note that the tropopause is often diagnosed with a lapse-rate criterion, and the two measures will often but not always be similar (Highwood & Hoskins, 1998), a point we return to later.

Writing – original draft: Brett A. McKim
Writing – review & editing: Brett A. McKim, Nadir Jeevanjee, Geoffrey K. Vallis, Neil T. Lewis

A longstanding approach to understanding the radiative tropopause is to use *gray* radiative transfer (independent of wavenumber) in the infrared, with a second gray band of radiation in the visible, and to couple a stratosphere in radiative equilibrium to a troposphere with a fixed lapse rate (Goody & Yung, 1989). Although such models were originally used to address planetary questions such as the runaway greenhouse effect (Nakajima et al., 1992), they have also been used to qualitatively study Earth's tropopause (Held, 1982; Thuburn & Craig, 2000) and its shifts under global warming (Vallis et al., 2015; Schneider & O'Gorman, 2008; Hu & Vallis, 2019). If in such gray models the stratosphere and upper troposphere are taken to be optically thin and in radiative equilibrium, then they become roughly isothermal at the planet's "skin temperature" (Pierrehumbert, 2010). The tropopause temperature T_{tp} is then just that skin temperature as dictated by the outgoing longwave radiation (OLR):

$$T_{tp} = (\mathrm{OLR}/2\sigma)^{1/4} \quad \text{(OLR constraint)}, \tag{1}$$

where σ is the Stefan-Boltzmann constant. This "OLR constraint" says that T_{tp} is tightly controlled by the radiative properties at the top of the atmosphere. The OLR constraint further implies that T_{tp} will be invariant under climate changes that do not change OLR (such as a change in gray optical depth), but will be sensitive to warming agents that increase OLR (such as an increase in insolation).

However, the relevance of the skin temperature in Equation 1 is a consequence of the gray assumption. Simply adding an infrared "window" to such gray models (so that part of the infrared spectrum is optically thin or even entirely transparent) is sufficient to at least partially decouple T_{tp} from the OLR, as shown by Hu and Vallis (2019). A further consequence is that "the stratospheric temperature is no longer independent of the existence of a troposphere, or of the tropopause height and thermal structure of the tropopause" (Pierrehumbert, 2010, Section 4.7).

The breakdown of the OLR constraint in more realistic settings and the possibility of greater tropospheric control over T_{tp} were highlighted by the cloud-resolving simulations of Seeley et al. (2019), which utilized spectral (wavenumber-dependent) radiative transfer and exhibited a Fixed Tropopause Temperature (FiTT) under surface warming, *without* fixed OLR. This result can be rationalized in terms of an entirely different paradigm focused on the fixed temperature of anvil clouds in response to surface warming (the Fixed Anvil Temperature (FAT) hypothesis, Hartmann & Larson, 2002). FAT says that tropical convection is tied to water vapor-driven radiative cooling (Harrop & Hartmann, 2012; Hartmann & Larson, 2002), where the latter is the primary source of radiative cooling in the troposphere (Manabe & Strickler, 1964). Moisture is thermodynamically constrained and declines exponentially with altitude and decreasing temperature, until there is so little water vapor that it can no longer radiatively cool, thereby limiting the vertical extent of convection and implying that convective anvil cloud tops should occur at a fixed temperature. This expectation has been validated across models and observations (Kuang & Hartmann, 2007; Kubar et al., 2007; Zelinka & Hartmann, 2010), and was also generalized to extratropical high clouds (Thompson et al., 2017; Thompson et al., 2019). Seeley et al. (2019) then suggested that similar reasoning may apply to the radiative tropopause, which can lie a few kilometers above anvil clouds; this argument was supported by Seidel and Yang (2022) who found that the temperatures of anvil clouds and the radiative tropopause co-vary with surface warming.

If this is all true, then the temperature dependence of water vapor and its tropospheric radiative cooling imposes a *moist thermodynamic constraint* on the tropopause, in contrast to the OLR constraint of Equation 1. It is also in contrast to Robinson and Catling (2014), who (albeit mainly considering dry planetary atmospheres) derive a constraint on tropopause pressure that requires the presence of shortwave absorption and a stratospheric temperature inversion to operate. However, this moist constraint has not yet provided precise predictions of T_{tp}, so the FiTT hypothesis lacks a quantitative basis. Also, while a moist gray model may be sufficient to produce a FiTT (Figure S1 of Seeley et al. (2019)), such a model by itself cannot resolve the tension between the OLR constraint and the tropopause behavior in simulations with spectral radiative transfer.

A way forward, however, may be found in the approach of Jeevanjee and Fueglistaler (2020b), who combined the usual moist thermodynamics with an analysis of water vapor spectroscopy to provide a quantitative theoretical foundation for FAT. Here, we take a similar approach but apply it to the radiative tropopause temperature and FiTT.

We begin in Section 2 by reviewing the theory of Jeevanjee and Fueglistaler (2020b) and the spectroscopy of water vapor to construct a constraint for T_{tp}. Sections 3 and 4 then validate this constraint against both single column as well as global simulations. We then connect the dots between the OLR constraint (Equation 1) and FiTT by demonstrating that a *moist* gray model simultaneously obeys FiTT and Equation 1, and that spectral radiation indeed breaks the connection between T_{tp} and OLR (Section 5).

Although we focus on the radiative tropopause (henceforth "the tropopause"), we will also touch on the lapse rate tropopause and the role of dynamical constraints (Stone & Carlson, 1979; Held, 1982; Schneider, 2004, 2008; Schneider and O'Gorman, 2008; O'Gorman, 2011; Zurita-Gotor & Vallis, 2011; Vallis, 2017). Stratospheric dynamics and ozone also affect tropopause structure (Birner, 2010; Dacie et al., 2019; Fueglistaler et al., 2009; Highwood & Hoskins, 1998; Lin et al., 2017; Thuburn & Craig, 2000, 2002), and their inclusion is necessary to capture the full complexity of the tropopause response to climate change (Randel & Jensen, 2013). We briefly consider the effects of ozone, but we primarily focus on more basic mechanisms that should be embedded in most climate models.

2. Formulating the Thermospectric Constraint

2.1. Qualitative Overview

Understanding clear-sky radiative cooling is key to constraining the tropopause. The cooling profile is controlled by the wavenumber-dependence of water vapor spectroscopy (Jeevanjee & Fueglistaler, 2020b). At each temperature (or height), there are only a limited range of wavenumbers that cool (Jeevanjee & Fueglistaler, 2020a, 2020b), with colder temperatures (higher heights) cooling at wavenumbers with stronger spectroscopic absorption. We demonstrate this in the Isca single column model (SCM) atmosphere with a surface temperature of $T_s = 290$ K (details of simulation in Section 3), and in a line-by-line radiative transfer, PyRADS (Koll & Cronin, 2018) with spectral data from the HITRAN 2016 database (Gordon et al., 2017). Plotting the spectrally-resolved cooling to space reveals that at any given height, most cooling is contained within a roughly 200 cm^{-1} width band whose contours mimic the V-shape of water vapor spectroscopy (Figures 1a and 1d).

Following this logic, water vapor's maximum mass absorption coefficient around 150 cm^{-1} (Figure 1a) suggests there is a minimum temperature (maximum height) to which water vapor can emit and radiatively cool to space (Figure 1b). This potentially constrains the radiative tropopause in terms of water vapor spectroscopy, along with Clausius-Clapeyron scaling which determines the vertical distribution of water vapor. We make these ideas precise in the next subsection.

2.2. Making the Constraint Quantitative

Small amounts of upper tropospheric water vapor can cool because of its strong radiative absorption in the rotational band (Figure 1a and Clough et al., 1992). Consider water vapor's optical depth:

$$\tau_{H_2O}(\nu, z) = \int_z^\infty \kappa_{H_2O}(\nu) \frac{p}{p_{ref}} \rho_{H_2O} dz', \tag{2}$$

where p is pressure, ρ_{H_2O} is water vapor density, $\kappa_{H_2O}(\nu)$ is the reference mass absorption coefficient of water vapor ($m^2\ kg^{-1}$) evaluated at wavenumber ν (cm^{-1}) and reference temperature $T_{ref} = 260$ K, pressure $p_{ref} = 500$ hPa, and p/p_{ref} accounts for the "pressure broadening" of κ_{H_2O} (Fu, 2006; Pierrehumbert, 2010; Romps et al., 2022). Deviations in κ_{H_2O} due to temperature are much smaller especially in the wavenumber range we consider (Figure S2 in Supporting Information S1), so we neglect this variation just as other studies do (Feng et al., 2023; Fildier et al., 2023; Jeevanjee & Fueglistaler, 2020b; Koll et al., 2023; Stevens & Kluft, 2023).

Infrared emission from water vapor peaks around $\tau_{H_2O} \approx 1$ (Jeevanjee, 2023; Jeevanjee & Fueglistaler, 2020a; Petty, 2006) and Figure 1d. For τ_{H_2O} to remain close to 1, variations in κ_{H_2O} must be compensated by the integral of ρ_{H_2O}. κ_{H_2O} varies by many orders of magnitude across the infrared (Figure 1a), so many possible values of z in Equation 2 can result in the product of κ_{H_2O} and the integral of ρ_{H_2O} being close to one. In other words, many atmospheric levels emit to space (Figures 1b and 1d). However, a maximum in κ_{H_2O} implies a minimum integral of ρ_{H_2O} and hence a maximum height z_{max} above which the atmosphere can no longer effectively cool to space.

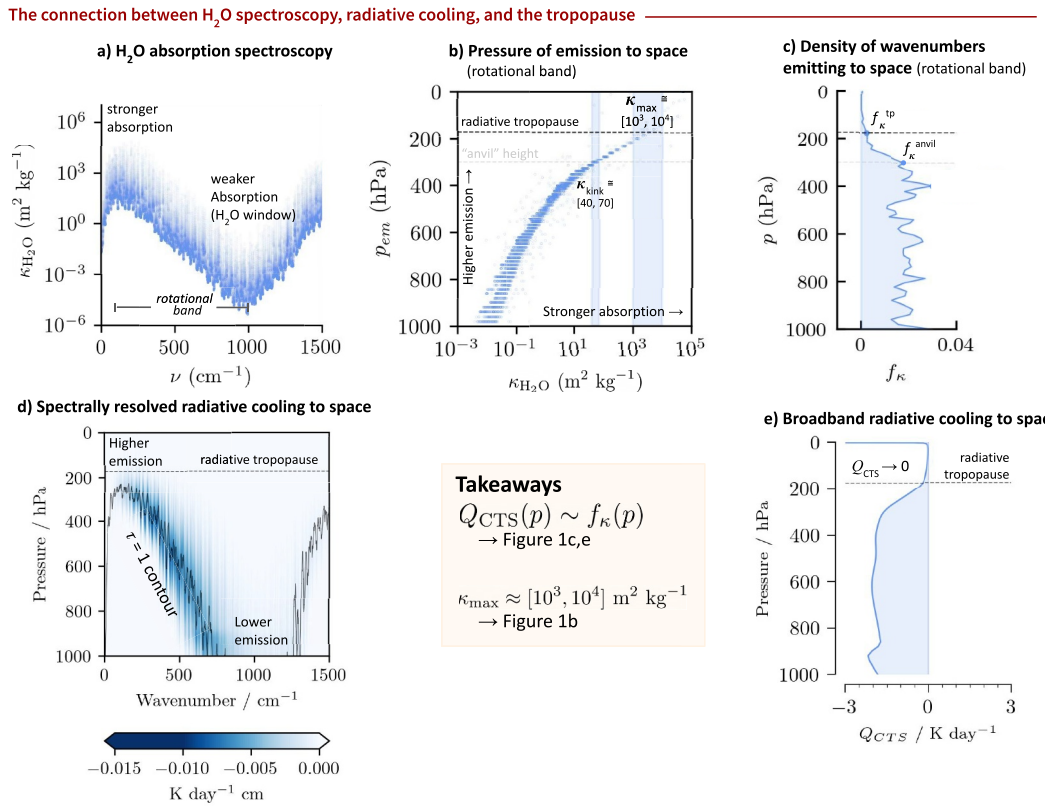

Figure 1. The max absorption strength of water vapor spectroscopic absorption is hypothesized to constrain Earth's tropopause temperature. (a) Water vapor reference mass absorption coefficients (κ_{H_2O}) evaluated at $p_{ref} = 500$ hPa and $T_{ref} = 260$ K as a function of wavenumber. (b) The emission pressure p_{em} as a function of the reference absorption coefficients of water vapor. κ_{max} is the plausible range of values (blue shading) for κ_{H_2O} at the radiative tropopause. $\kappa_{kink} = 40 - 70$ m^2 kg^{-1} refers to where the density of lines begins to decline rapidly, which has been hypothesized to relate to anvil clouds (Jeevanjee & Fueglistaler, 2020b). (c) The wavenumbers emitting to space at a given height, divided by the total number of wavenumbers in the rotational band. (d) Spectrally-resolved longwave radiative cooling to space from the Isca single column model (SCM) control run with off-line line-by-line radiative transfer calculated with PyRADS. (d) Spectrally-integrated longwave radiative cooling to space (Q_{CTS}). (Notes) We make a rough estimate of the maximum absorption coefficient as $\kappa_{max} \sim 10^3 - 10^4$ m^2 kg^{-1}, which we hypothesize relates to the tropopause. Spectral data computed at a resolution of 0.1 cm^{-1} using PyRADS (Koll & Cronin, 2018). The spectrally resolved radative cooling in (c) is plotted after averaging results to 10 cm^{-1} resolution. The κ_{H_2O} distribution is insensitive with respect to increased computational resolution (0.01 cm^{-1}) and the radiative cooling is insensitive with respect to assumptions of line shape (Lorentz and Voigt), see Figure S8 in Supporting Information S1.

Owing to the Clausius-Clapeyron scaling $\rho_{H_2O} \sim \exp(-L/R_v T)$, this constraint can be more easily expressed as a minimum atmospheric temperature that efficiently cools radiatively to space.

To formulate this statement quantitatively, we assume that all emission occurs at $\tau_{H_2O} = 1$, which lets us define an emitting temperature T_{em} at wavenumber ν by the relation

$$\tau_{H_2O}(\nu, T_{em}) = 1. \tag{3}$$

As detailed in Appendix A, one can evaluate the integral in Equation 2 and then invert Equation 3 analytically to obtain T_{em} as a function of κ_{H_2O}:

$$T_{em}(\kappa_{H_2O}) = \frac{T^*}{W\left(\frac{T^*}{T_{ref}}(D \cdot \mathrm{RH} \cdot M_v \cdot \kappa_{H_2O})^{R_d \Gamma / g}\right)}. \tag{4}$$

Here, W is the Lambert-W function which inverts the function $y = x\exp(x)$, T_{ref} is the temperature at $p_{\text{ref}} = 500$ hPa (which is where the T_s-dependence of T_{tp} is accounted for), relative humidity (RH) is the column RH, and the other parameters and constants in this equation are described in Appendix A; we write out Equation 4 here mainly for concreteness, and to emphasize that an explicit, analytic formulation is possible. This can also be calculated numerically, which we do when plotting the emission pressure p_{em} in Figure 1b.

We now posit that the tropopause temperature T_{tp} is simply the emission temperature (Equation 4) evaluated at a suitable maximum H_2O absorption coefficient κ_{max}, that is,

$$T_{\text{tp}} = T_{\text{em}}(\kappa_{\text{max}}). \quad \text{(Thermospectric constraint)} \tag{5}$$

We refer to this as a "thermospectric constraint" as it combines water vapor spectroscopy (via κ_{max}) with the thermodynamic Clausius-Clapeyron scaling implicit in Equation 4, where the Lambert W function inverts the $\exp(-L/R_vT)$ factor in H_2O optical depth (Equation A1).

The presence of thousands of absorption lines across the infrared (Figure 1a) and the multiplicity of absorption coefficients that correspond to emission at the tropopause (Figure 1b) makes the value of κ_{max} ambiguous. But, this ambiguity actually corresponds to the ambiguity in choosing a radiative cooling threshold to define the radiative tropopause. To see this, we modify Equation 17 of Jeevanjee and Fueglistaler (2020b) to approximate the spectrally integrated radiative cooling to space profile Q_{CTS} (K day^{-1}) in terms of the density of wavenumbers in the rotational band emitting at a given height, $f_\kappa(p)$:

$$Q_{\text{CTS}}(p) = -\frac{g}{c_p}\pi B(\nu_{\text{em}}, T(p))\frac{\beta}{p}f_\kappa(p)\Delta\nu_{\text{rot}}. \tag{6}$$

Here $\Delta\nu_{\text{rot}} = 850$ cm^{-1} is the spectral width of the H_2O rotational band: $\nu \in [150, 1000]$ cm^{-1}, $B(\nu_{\text{em}}, T(p))$ is the Planck function evaluated at the center of the rotational band ($\nu_{\text{em}} = 575$ cm^{-1}), and $\beta = d\log\tau_{H_2O}/d\log p \approx 5$. Equation 6 follows from Equation 17 of Jeevanjee and Fueglistaler (2020b) by noting that their spectroscopic decay parameter $l = (d\ln\kappa_{H_2O}/d\nu)^{-1}$ is just the wavenumber range per unit ln κ_{H_2O}, which they assumed was constant throughout the spectrum but which in general equals $f_\kappa(p)\Delta\nu_{\text{rot}}$ by the definition of $f_\kappa(p)$.

Equation 6 implies $Q_{\text{CTS}}(p) \propto f_\kappa(p)$ and the correspondence between Figures 1c and 1e confirms this. The decline in $f_\kappa(p)$ at large κ_{H_2O} in the upper troposphere is closely related to the decline in radiative cooling in the upper troposphere, and ambiguity in specifying a small threshold value for the radiative cooling for defining the radiative tropopause corresponds naturally to ambiguity in determining κ_{max} (Figure S4 in Supporting Information S1). In the next section, we will specify a threshold for the total radiative cooling Q, use this to determine κ_{max} via optimization with respect to a control simulation, and then test the thermospectric constraint (Equation 4) by varying other parameters in Equation 4.

In the meantime, however, we can make a rough, heuristic estimate of T_{tp} by assuming a radiative cooling threshold between a tenth and a hundredth of its tropospheric value of -1.5 K day^{-1}, which by Equation 6 should correspond to f_κ dropping to between 1/10 and 1/100 of its tropospheric value of 0.02 $(\ln\kappa_{H_2O})^{-1}$. One might then reasonably assign κ_{max} to be anywhere between $\left(10^3, 10^4\right)$ m^2 kg^{-1}, yielding via Equation 4 a T_{tp} between 182 and 195 K, a reasonable estimate as we will soon see. This heuristic (and assuming $\rho_{H_2O} \sim \exp(-L/R_vT)$ everywhere in deriving the thermospectric constraint) relies on the observation that stratospheric water vapor does not produce much radiative cooling to space (Figure 1d) in our control simulation. The potential role of stratospheric moisture on the tropopause temperature is discussed in the SI.

3. Testing the Thermospectric Constraint

To more precisely test the thermospectric constraint (Equation 5), we run simulations using a clear-sky SCM configuration of the Isca modeling framework (Vallis et al., 2018). The SCM is configured with the correlated-k rapid and accurate radiative transfer model (RRTM) (Mlawer et al., 1997), a boundary layer turbulence profile scheme similar to Troen & Mahrt, 1986, and a simplified representation of moist convection (the simple Betts-Miller code of Frierson, 2007; O'Gorman & Schneider, 2008). In a single column context, the simple Betts-Miller

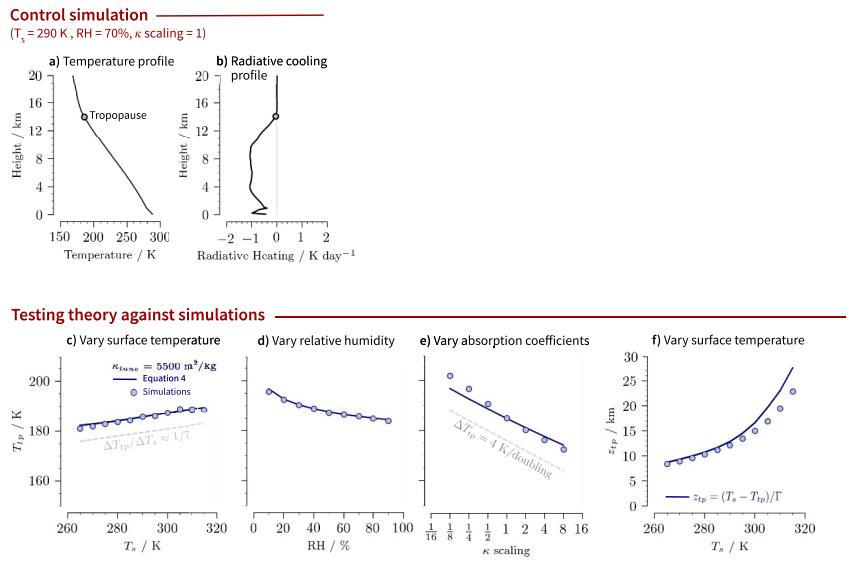

Figure 2. The thermospectric constraint, Equations 4, 5 and 8, can quantitatively capture the change in tropopause temperature (T_{tp}) and height (z_{tp}) across a wide range of climates. (a) Isca's SCM control simulation's temperature profile. (b) Control simulation's radiative cooling profile. (c) The surface temperature is varied and relative humidity (RH) kept fixed at 0.7. Simulations (blue dots), theory (solid blue lines), and scaling arguments (dashed gray lines). (d) The RH is varied and T_s fixed at 290 K. (e) The absorption coefficients of water vapor are scaled uniformly and T_s and RH are fixed at 290 K and 0.7, respectively. (f) Tropopause height as a function of surface temperature. Γ is the average lapse rate between the surface and the tropopause. Water vapor and CO_2 (280 ppmv) are the only greenhouse gases present in these simulations.

convection scheme essentially constrains the atmospheric temperature profile to a moist adiabat, but in a general circulation model (GCM) where horizontal transfers of energy can occur, deviations from the moist adiabat should be expected, particularly in the extratropics. Configuring the SCM using Isca lets us compare to GCM simulations with identical column-wise physics (but additional horizontal processes) later in the paper. Further description of our model set-up can be found in the Supporting Information.

To begin, we consider an SCM control run with a prescribed surface temperature of $T_{\mathrm{s}} = 290$ K, RH= 0.7, and CO_2 concentration of 280 ppmv. The diagnosed tropopause temperature is 186 K when using the -0.05 K day^{-1} net radiative cooling threshold. The choice of threshold affects the climatological value of T_{tp} (consistent with the ambiguity in choosing κ_{max}), but it does not affect the trend in T_{tp} with surface warming (Figure S4 in Supporting Information S1).

κ_{max} can be determined via optimization by matching the predicted tropopause temperature from Equations 4 and 5 with the value diagnosed from the SCM control (186 K). Optimizing κ_{max} results in a value of 5500 m^2 kg^{-1}, which is within our identified range for κ_{max} based on the density of absorption lines $f_\kappa(p)$. (This value is used henceforth and will not be re-tuned, except where explicitly scaled so as to compare to numerical experiments where the absorption coefficients of water vapor are explicitly scaled.) Regarding this climate as our base state, we can test the thermospectric constraint by varying the prescribed surface temperature, column RH, and absorption coefficients of water vapor in the SCM and see how well theory compares with the numerical simulations.

3.1. Surface Temperature

As surface temperature increases, the thermospectric constraint (Equation 5) predicts a small but nonzero warming of the tropopause (Figure 2c, solid line). Physically, the slight warming can be understood as follows. The tropopause temperature is fixed, to lowest order, which implies a rising tropopause as surface temperature increases. As pressure decreases, the effective water vapor absorption coefficients $\left(\kappa_{\mathrm{H_2O}} \cdot p/p_{\mathrm{ref}}\right)$ also decreases, which implies a larger integral of $\rho_{\mathrm{H_2O}}$ is needed to achieve $\tau_{\mathrm{H_2O}} = 1$ (Equation 2), and thus a slightly warmer tropopause temperature (assuming fixed RH). Algebraically, the slight warming can be calculated implicitly as shown by Jeevanjee, 2023, by combining Equations A1 and A2 and doing some algebra:

$$\frac{dT_{\mathrm{tp}}}{dT_s} = \frac{T_{\mathrm{tp}}}{T_s}\frac{1}{\frac{LR_d\Gamma}{gR_vT_{\mathrm{tp}}} - 1} \approx 1/7. \tag{7}$$

In an SCM experiment where surface temperature is increased (Figure 2c, dots), the tropopause warms almost exactly as predicted. Thus, in the context of our idealized modeling framework, the thermospectric constraint provides a quantitative understanding of how T_{tp} should change with warming, buttressing the qualitative expectations of a FiTT (Seeley et al., 2019; Thompson et al., 2019) from purely thermodynamic constraints. Note that our explanation of slight changes in tropopause temperature as a consequence of pressure broadening effects differs from Hu and Vallis (2019), who explains the slight warming as a consequence of increased longwave radiation from outside the water vapor window. We attempt to reconcile these two theories of tropopause temperature in Section 5.

Tropopause height is found to increase with surface temperature (Figure 2d), consistent with more comprehensive models and observations (Lorenz & DeWeaver, 2007; Santer et al., 2003; Schneider et al., 2010; Vallis et al., 2015). We are able to predict this rise if we permit ourselves to take the vertically averaged tropospheric lapse-rate, Γ, as an input:

$$z_{tp} = \frac{T_s - T_{\mathrm{tp}}}{\Gamma}. \tag{8}$$

This simple constraint captures the increase in tropopause height with surface warming (Figure 2f), similar to studies employing gray radiation in their theory for tropopause height (Thuburn & Craig, 2000; Schneider & O'Gorman, 2008; Vallis et al., 2015; Hu & Vallis, 2019). However, our theory provides a more predictive and comprehensive understanding of tropopause temperature itself and need not rely on any planetary energy balance argument (i.e., the OLR) to constrain z_{tp}.

3.2. Relative Humidity

Variations in column RH may influence T_{tp}. A larger RH implies a smaller integral of saturation water vapor density $\rho^{\mathrm{sat}}_{H_2O}$ required to reach $\tau_{H_2O} = 1$, and thus a cooler temperature. We vary RH in the SCM but keep surface temperature fixed and find that the tropopause cools as RH increases (Figure 2d), in excellent agreement with predictions from inputting RH into the thermospectric constraint (Equation 4).

3.3. Water Vapor Absorption

Thermodynamic constraints suggest that modifying the ρ_{H_2O} passed to the radiative transfer code of a climate model alters the temperature of anvil clouds and the tropopause, which is indeed the case across a spectrum of models (Harrop & Hartmann, 2012; Spaulding-Astudillo & Mitchell, 2023; Thompson et al., 2019). The thermospectric constraint suggests that uniformly scaling the absorption coefficients κ_{H_2O} in lookup tables passed to the RRTM radiative transfer calculation (e.g., Mlawer et al., 1997) should have a similar effect. A geometrically larger $\kappa_{\max}$ implies a geometrically smaller minimum integral of ρ_{H_2O} to achieve $\tau_{H_2O} = 1$ and hence an arithmetically colder T_{tp} due to Clausius-Clapeyron scaling: $d\ln\rho_{H_2O}/dT|_{T_{\mathrm{tp}}} = L/\left(R_vT^2_{\mathrm{tp}}\right) = 16\%\ \mathrm{K}^{-1}$ or roughly 4 K of cooling to halve ρ_{H_2O}. These predictions are borne out quantitatively by the simulations, where T_{tp} cools arithmetically as $\kappa_{\max}$ is scaled geometrically over many octaves while T_s and RH are fixed, at a rate of roughly 4 K per doubling (Figure 2e). This is the most direct test of the thermospectric constraint and it confirms spectroscopy's key role in constraining T_{tp}.

4. From Spectroscopy to the General Circulation

The previous tests were done in a SCM, but the tropopause is a feature of Earth's general circulation and may be influenced by non-column wise dynamics (Birner, 2010; Thuburn & Craig, 2000). We will therefore test for a FiTT by modifying the surface temperature in a GCM configured as an idealized aquaplanet with a standard fixed sea surface temperature (SST) distribution (Neale & Hoskins, 2000):

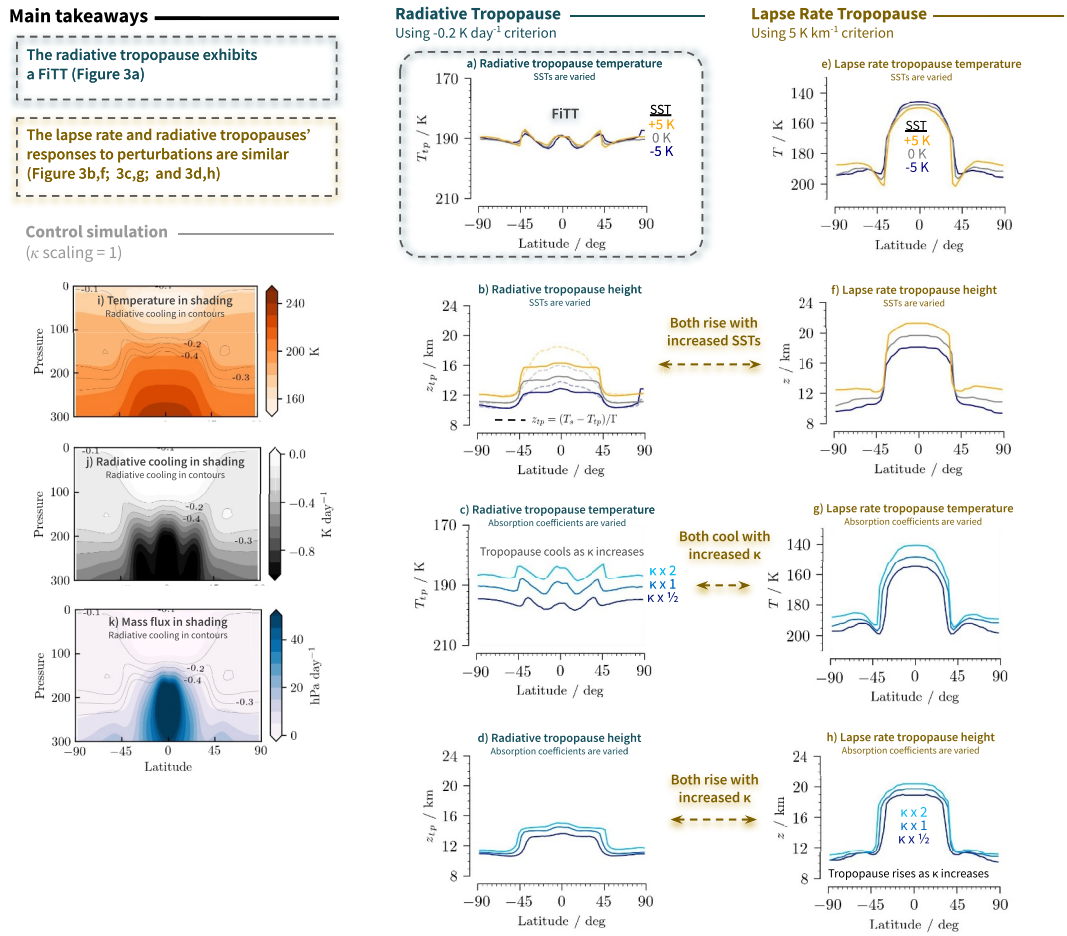

Figure 3. The radiative tropopause exhibits a Fixed Tropopause Temperature (FiTT) and the lapse-rate tropopause's responses to perturbations are qualitatively, if not quantitatively, similar to the radiative tropopause in many cases. (a), (e) Radiative and lapse rate tropopause temperature for the Isca aquaplanet simulations with sea surface temperatures uniformly perturbed by −5, 0, and 5 K. (b), (f) Radiative and lapse rate tropopause height for the same set of simulations. The constraint on tropopause height (Equation 8) is plotted with the dashed lines in (b). T_s, T_{tp}, and Γ are diagnosed from the simulations. (c), (g) Radiative and lapse rate tropopause temperature for the general circulation model simulations in which the water vapor absorption coefficients κ_{H_2O} are perturbed geometrically by [1/2, 1, 2]. (d), (h) Radiative and lapse rate tropopause height for the same set of simulations. The lack of ozone in these simulations accounts for the high (≈ 20 km) lapse rate tropopause. (i) Zonal-mean temperature profile of the control Isca aquaplanet simulation. (j) Zonal-mean radiative cooling profile of the control. (k) Zonal-mean mass flux profile of the control.

$$T_s(\phi) = \begin{cases} 300\left(1 - \sin^2(3\phi/2)\right)\ \text{K}, & \text{for } -\pi/3 < \phi < \pi/3 \\ 273\ \text{K}, & \text{otherwise}, \end{cases} \tag{9}$$

where ϕ is the latitude. We will then directly test the role of spectroscopy by modifying κ_{H_2O} and seeing if it influences T_{tp} and z_{tp} (tropopause height).

The GCM is configured to use the same column-wise physics routines (e.g., RRTM radiative transfer, simplified Betts-Miller moist convection) as the SCM. See the Supporting Information S1 for further details. When analyzing the GCM, we diagnose the radiative tropopause with a -0.2 K day^{-1} threshold instead of the -0.05 K day^{-1} used for the SCM. The updated threshold more closely aligns with relevant dynamical features such the mass flux profile (Figure 3k) while still using a threshold value ≪ typical tropospheric cooling (Figure 3j). If one were to keep using the -0.05 K day^{-1} threshold, then the radiative tropopause would be very high in the

atmosphere, where it no longer aligns with the dynamical features of the atmosphere (Figures 3j and 3k). Again, this ambiguity in a specific threshold of cooling mirrors the ambiguity in determining $\kappa_{\max}$.

4.1. The Radiative Tropopause

We vary the surface temperatures $T_s(\phi)$ by uniform perturbations of ±5 K and find that the tropopause temperature remains fixed to within ±1 K (Figure 3a). In addition, if we look at T_{tp} as a function of latitude, we find that it only varies by 5 K from the equator to poles. The invariance in T_{tp} with respect to global T_s and across latitude confirms the robustness of FiTT in a more comprehensive model. Looking at tropopause height at a given latitude, we find that z_{tp} rises as global T_s increases (Figure 3b), in general agreement with Equation 8 (dashed lines). Furthermore, the rough agreement with Equation 8 shows that much of the meridional variation in tropopause height can be attributed to meridional variations in T_s and the vertically averaged lapse rate, Γ.

We next consider GCM simulations where we vary κ_{H_2O} geometrically. We find the tropopause cools and rises across all latitudes as κ_{H_2O} increases, again at $\approx 4 - 5$ K and $0.5 - 1$ km per doubling of κ_{H_2O} (Figures 3c and 3d). This cooling confirms the quantitative predictions of thermospectric constraint (Figure 2e) in a more comprehensive and Earth-like setting.

4.2. The Lapse Rate Tropopause

The tropopause is also often diagnosed via a lapse-rate criterion (WMO, 1957), taken here as the height above which the lapse rate exceeds 5 K km^{-1}. Thus defined, the lapse-rate tropopause has a much more pronounced top-hat structure in both its height and temperature (Figures 3e and 3f), due to the more pronounced influence of latitudinally varying dynamics and stratospheric circulation (Schneider & O'Gorman, 2008; Haqq-Misra et al., 2011; Birner, 2010). But, even though the dominant dynamics shifts from moist convection to baroclinic eddies as one moves poleward (Held, 1982; Schneider, 2008; Stone & Carlson, 1979; Vallis, 2017), the heating from these dynamics must be balanced by radiative cooling, so one may nonetheless expect the lapse rate tropopause to behave similarly to the radiative tropopause in some respects.

Indeed, when $T_s(\phi)$ is uniformly perturbed by ±5 K, we find that the lapse rate and radiative tropopauses both rise by comparable amounts (Figures 3b and 3f). Furthermore, when κ_{H_2O} is increased geometrically we find that both tropopauses cool and rise, again by roughly comparable amounts (Figures 3c and 3g and 3h). This latter observation confirms the influence of H_2O spectroscopy on tropopause height and temperature across multiple definitions of the tropopause.

At the same time, however, the temperature of the lapse rate tropopause does not appear to be as tightly constrained by moist thermodynamics as that of the radiative tropopause, as it varies much more as a function of latitude and also responds more noticeably to variations in surface temperature (Figure 3e). FiTT, then, does not apply to all definitions of the tropopause, presumably because each definition respects different physical constraints and can respond in different ways to changes in forcing (Fueglistaler et al., 2009; Highwood & Hoskins, 1998). Nevertheless, the many similarities in the behavior of these two definitions of the tropopause suggest that much of what one learns about the radiative tropopause may apply to the lapse rate tropopause as well.

4.3. Other Controls of the Radiative Tropopause

Small meridional variations in radiative tropopause temperature may be due to surface temperature, which varies between 300 and 273 K from equator to poles and can change T_{tp} with pressure-broadening effects. They may also be due to tropospheric RH, which varies from 20 to 70 % (Figure S1a in Supporting Information S1). The SCM and Equation 4 shows varying column RH by a similar amount changes T_{tp} by about 5 K (Figure 2d). The lapse rate (Figure S1b in Supporting Information S1) could also change T_{tp}; changing Γ from 4 K km^{-1} to 7 K km^{-1} in Equation 4 changes T_{tp} by 3 K.

Stratospheric moisture could also in principle influence the radiative tropopause, since it is well known to modulate Earth's top of atmosphere radiation (Dessler et al., 2013; Solomon et al., 2010). However, the stratosphere in our single column simulations is colder and drier ($q_v^{\text{strat}} = 10^{-7}$ kg kg^{-1}) than observed ($q_v^{\text{strat}} = 2 \times 10^{-6}$ kg kg^{-1}, Fueglistaler et al., 2009) due to the lack of ozone. Running the SCM with a specified ozone profile results in an increase in stratospheric cooling, consistent with previous studies such as Clough

et al., 1992 (Figure S10 in Supporting Information S1). It is thus important to test whether including a realistic amount of stratospheric moisture changes our argument that where $f_\kappa(p)$ approaches zero is well aligned with the radiative tropopause (Figures 1c and 1e). We do this by imposing an Earth-like value of q_v^{strat} in the offline line-by-line radiation transfer calculation (Figure S9 in Supporting Information S1). We find that increasing stratospheric water vapor from 10^{-7} kg kg^{-1} to 2×10^{-6} kg kg^{-1} reduces the OLR by ≈ 1 Wm^{-2} via small increases in stratospheric optical depth and stratospheric radiative cooling. This gives rise to slight changes in $f_\kappa(p)$, but its value at the tropopause is still suppressed by at least an order of magnitude relative to its tropospheric values, consistent with our argument that where $f_\kappa(p) \to 0$ aligns with the diagnosed radiative tropopause in the control simulation. Thus, we expect that including this stratospheric moisture in our calculation of the tropopause temperature (Equation 5) could cause only a small quantitative change, but not a qualitatively different one. Further discussion of this topic can be found in Supporting Information S1.

Column-wise physics and stratospheric water vapor may not be the only source of variations in T_{tp}. Stratospheric dynamics may influence z_{tp} and T_{tp} by altering the location of zero radiative cooling (Birner, 2010; Hu & Vallis, 2019; Thuburn & Craig, 2000). CO_2-driven radiative cooling, which primarily emanates from the stratosphere (Jeevanjee & Fueglistaler, 2020b), may also drive changes in T_{tp}. Future work could address these questions and lead to a more comprehensive theory, but our goal here is to provide a lowest-order picture of how moist thermodynamics interacting with spectroscopy constrains the radiative tropopause and its change with warming.

5. Reconciling Different Constraints

Previous theories of tropopause temperature have either emphasized outgoing radiation (Held, 1982; Thuburn & Craig, 2000; Vallis et al., 2015) *or* moist thermodynamics and upper tropospheric radiative cooling (Hartmann & Larson, 2002; Thompson et al., 2017). As mentioned in the introduction, these constraints can lead to different conclusions about the change in tropopause temperature with warming. Here, we seek to better understand the following:

1. Under what circumstances does FiTT apply?
2. Under what circumstances does the OLR constraint (Equation 1) apply?

To answer these questions, we will compare and contrast the behavior of OLR and tropopause temperature in an experiment where the surface temperature is varied in suite of climate models: a "dry" gray SCM in Isca without any coupling of moisture to radiation, similar to Frierson et al. (2006); a "moist" gray model with radiatively interactive moisture, similar to Byrne and O'Gorman (2013); and a spectral model with radiatively interactive moisture, which has already been used in this paper.

In this experiment, we find that the models with radiatively interactive moisture exhibit a FiTT. That is, the diagnosed tropopause temperature from the radiative cooling profile does not change much compared to the surface temperature (see the circles connected with solid lines in Figures 4b and 4c). There is some slight warming in the spectral simulations due to the previously mentioned pressure broadening of water vapor absorption. In contrast, the model without radiatively interactive moisture does not exhibit a FiTT (Figure 4a).

We also find that gray models with a single band of radiation follow the OLR constraint (Figures 4a and 4b), which is indicated by the tight correspondence between T_{tp} diagnosed from the radiative cooling profile (circles connected by solid lines) and T_{tp} diagnosed from the OLR constraint in Equation 1 (squares connected by dashed lines). In contrast, the model with spectral radiative transfer (and radiatively interactive moisture) does not follow the OLR constraint (Figure 4c).

Why does T_{tp} vary with surface temperature in the dry case, but remains roughly constant in the moist cases? In dry simulations, the greenhouse gas is assumed to be well mixed and so optical depth is a single valued function of pressure, $\tau = \tau(p)$. As T_s increases, isobars warm and radiative cooling at $\tau = 1$ emanates from a warmer layer of atmosphere (Figure 4d). In simulations with radiatively-coupled moisture, however, the optical depth is constrained by Clausius–Clapeyron scaling to be a single valued function of temperature, $\tau = \tau(T)$ (in the absence of pressure broadening). As T_s increases, radiative cooling at $\tau = 1$ emanates from nearly the same temperature (Figure 4e and 4f and Figure S1a of Seeley et al., 2019) and T_{tp} is roughly constant.

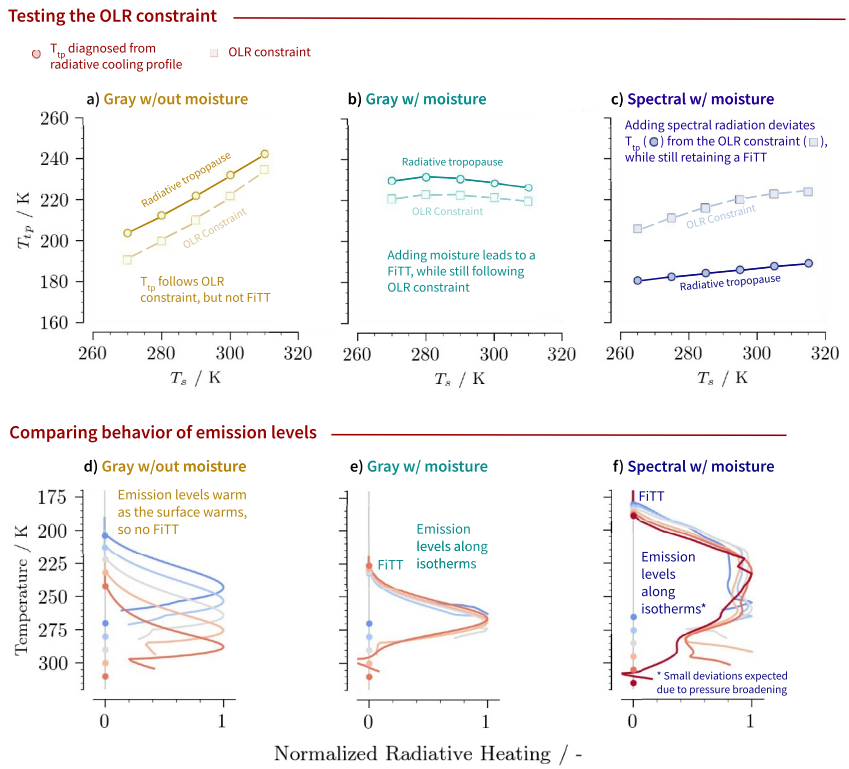

Figure 4. Moisture is essential to capturing a FiTT and spectral radiative transfer decouples tropopause temperature from outgoing longwave radiation (OLR). Surface temperature is varied in the Isca SCM from 270 to 310 K for climate models with dry gray, moist gray, and spectral radiative transfer. (a) Tropopause temperature diagnosed from the OLR constraint (squares, Equation 1) and from the radiative cooling threshold (circles) for gray simulations without radiatively active moisture. (b) Same, but for moist gray simulations. (c) Same, but for spectral moist simulations. (d)–(f) The radiative cooling profile plotted in temperature coordinates for each set of simulations. Each profile has been normalized by its maximum tropospheric value and is plotted starting at the lifting condensation level for clarity. See Supporting Information S1 for details.

As for Question 2, how can T_{tp} decouple from OLR in the model with spectral radiation? Pierrehumbert (2010, Section 4.7) suggested and Hu and Vallis (2019) showed that adding an optically thin "window" band to a gray model decouples the radiative equilibrium temperature of the upper atmosphere from total OLR and couples it instead to outgoing radiation from the optically thick band (OLR_{thick}). This results in a weaker constraint on tropopause temperature,

$$T_{tp} = \left[\frac{OLR_{thick}}{2\sigma}\right]^{1/4} \quad \text{(when there is an infrared window).} \tag{10}$$

While the window band's emission contributes to the OLR, it drops out in Equation 10 because this band becomes optically thin at the surface, so its emission cannot contribute to radiative balance at the tropopause (Hu & Vallis, 2019). In fact, it is only the most optically thick bands that determines radiative balance at the tropopause. In the spectral limit where many bands (i.e., wavenumbers) and optical thicknesses are considered, T_{tp} is just the brightness temperature of the emission from the most optically thick band set by κ_{max}. This is essentially what we have calculated with the thermospectric constraint (Equations 4 and 5).

To summarize: radiatively interactive moisture produces a FiTT, and gray radiation constrains T_{tp} in terms of OLR. This is why simulations employing spectral radiative transfer with radiatively interactive moisture get a FiTT despite a changing OLR (Seeley et al., 2019; Seidel & Yang, 2022, and Figure 4c and Figure S7 in Supporting Information S1). This is also true for such simulations where the SST is varied by increased insolation, in

which the top of atmosphere energy balance is respected (Figure S6 in Supporting Information S1). On the other hand, the fact that the OLR constraint on T_{tp} only holds for gray radiation models suggests that this constraint is somewhat artifactual in the sense that it should not be expected to quantitatively hold in comprehensive models or in nature.

6. Discussion

6.1. Summary

Spectral radiative transfer decouples Earth's radiative tropopause temperature from the total outgoing radiation and, in a moist atmosphere, constrains it instead to where water vapor becomes optically thin across *all* wavenumbers and stops radiative cooling. This is set by water vapor's maximum spectroscopic absorption and Clausius-Clapeyron scaling. The thermospectric constraint implies a relatively fixed radiative tropopause temperature (FiTT) with warming because isopleths of water vapor path follows isotherms. However, pressure broadening modifies the strength of spectroscopic absorption as the tropopause rises with surface warming, causing it to warm slightly. FiTT also constrains the radiative tropopause to a constant temperature across latitude, and both the radiative and lapse rate tropopauses are strongly influenced by the strength of water vapor's absorption coefficients.

The thermospectric constraint does not rule out a role for processes such as the Brewer-Dobson circulation (which is relatively weak in an aquaplanet, but can affect the tropopause height; Thuburn & Craig, 2000; Birner, 2010; Hu & Vallis, 2019) and ozone (which can affect stratospheric temperature; see Figure S5 in Supporting Information S1 and Manabe & Strickler, 1964; Thuburn & Craig, 2000, 2002; Lin et al., 2017; Dacie et al., 2019), but it does suggest that a previously unnoticed mechanism grounded in robust physics is important in controlling tropopause temperature. This mechanism is qualitatively different from the idea that stratospheric properties and constituents primarily control the tropopause, (e.g., Goody & Yung, 1989), which is derived in terms of matching tropopause fluxes in a gray radiation model, similar to how the OLR constraint is derived. Therefore, perhaps it is not surprising that our results contest some of the predictions from stratospheric control, for instance, the tropopause pressure being constrained to roughly 100 hPa in a dry atmoshere (Robinson & Catling, 2014). We find that the tropopause rises by a factor of 5 from 286 hPa to 48 hPa just by varying the surface temperature in the SCM from 265 to 315 K, (Figure S3 in Supporting Information S1). In contrast, tropopause temperature varies by less than 10%. Presumably, our results differ from Robinson and Catling (2014), who were focused on dry planetary atmospheres, due to their constraint's assumption of gray radiation, a dry greenhouse gas, and their requirement of a stratospheric inversion.

6.2. Anvil Clouds and the Tropopause

The temperature of anvil clouds and the tropopause respond similarly to surface warming (Seidel & Yang, 2022), despite their roughly five km difference in height (Seeley et al., 2019). The thermospectric constraint offers an explanation. Anvil clouds and the tropopause share a thermodynamic control by water vapor, which is why they respond similarly to warming, but they depend on distinct features of water vapor spectroscopy, so they occur at different temperatures. The radiative tropopause occurs where radiative cooling goes to zero, which is controlled by the maximum spectroscopic absorption ($\kappa_{max} \approx 5500\ m^2\ kg^{-1}$): $T_{tp} = T_{em}(\kappa_{max}) \approx 186$ K. Anvil clouds predominantly occur near the max vertical derivative of radiative cooling (Hartmann & Larson, 2002), which is controlled by the *sharp decline* in water vapor's emission line density at $\kappa_{kink} = 40 - 70\ m^2\ kg^{-1}$ (Figures 1b and 1c): $T_{anvil} = T_{em}(\kappa_{kink}) \approx 214$ K (see also Jeevanjee & Fueglistaler, 2020b). These thermodynamic and spectroscopic ingredients are well represented in most climate models, which could be expected to be robust across a variety of modeling choices, including surface temperature, greenhouse gas concentration, and the representation of radiative transfer (e.g., Seidel & Yang, 2022).

6.3. A Role for Gray Radiative Transfer in Studying Climate?

Water vapor's thermodynamic and radiative properties have distinct but equally profound influences on Earth's climate (Held & Soden, 2006; Stevens & Bony, 2013); are gray models of radiative transfer fit for understanding these influences? In some cases, yes. Gray climate models can capture the interplay of latent heat release and the general circulation under global warming (Frierson et al., 2006; Schneider et al., 2010; Vallis, 2020), some of the

interaction between radiation and moisture necessary for water vapor feedbacks (Byrne & O'Gorman, 2013) and the runaway greenhouse effect (Nakajima et al., 1992), and they can offer a qualitative understanding of Earth's greenhouse effect (Pierrehumbert, 2010).

At the same time, some studies have shown that the circulation response is sensitive to the choice of gray versus spectral radiation (Kang et al., 2009; Tan et al., 2019). Furthermore, the spectral approach has recently yielded new quantitative understanding for a host of basic climate phenomena, such as the forcing from CO_2 (He et al., 2023; Jeevanjee et al., 2021), water vapor feedback (Feng et al., 2023; Koll et al., 2023), equilibrium climate sensitivity (Jeevanjee, 2023; Stevens & Kluft, 2023), and the temperatures of anvil clouds (Hartmann & Larson, 2002; Jeevanjee & Fueglistaler, 2020b) and congestus clouds (Spaulding-Astudilo & Mitchell, 2025). In these cases, radiation's wavenumber dependence has proven essential. It could be useful to revisit other results obtained with gray models, including those obtained in a planetary atmosphere context (Parmentier & Guillot, 2014; Rauscher & Menou, 2012; Robinson & Catling, 2014), to see if a spectral approach can provide additional insight there as well.

Appendix A: Water Vapor Optical Depth

The variable of integration in Equation 2 can be changed from height to temperature, and though $\kappa_{H_2O}\, p/p_{ref}$ varies due to pressure broadening, it varies much less than water vapor density does across the troposphere, so it can be pulled out of the integral. Optical depth is then proportional to water vapor path, which can be computed analytically (Koll & Cronin, 2018), resulting in a simplified expression:

$$\tau_{H_2O}(\kappa_{H_2O}, T) \approx \underbrace{\kappa_{H_2O}\frac{p}{p_{ref}}}_{\text{spectroscopy}} \underbrace{M_v \mathrm{RH} \exp\left(-\frac{L}{R_v T}\right)}_{\text{water vapor path}}, \tag{A1}$$

where $M_v \equiv p_v^{ref} T_{av}/\Gamma L$ is a characteristic column water vapor mass (kg m^{-2}), where $T_{av} \equiv (T_s + T_{tp})/2$, which we set to a constant of 250 K for simplicity (results are not sensitive to this approximation), $p_v^{ref} = 2.5 \times 10^9$ hPa is a reference pressure from Clausius-Clapeyron scaling, $L = 2.5 \times 10^6$ J kg^{-1} is water's latent heat of vapourization,and $M_v \mathrm{RH} \exp(-L/R_v T)$ is the column mass of water vapor above the isotherm with temperature T. The stratospheric contribution to water vapor optical depth can be ignored since $\tau_{strat} \ll 1$ and the density of wavenumbers emitting to space $f_\kappa \ll 1$ in the stratosphere (Figure S9 in Supporting Information S1, second and third row, respectively); further discussion of stratospheric moisture is presented in the SI and an abbreviated discussion is presented later in the main text.)

Setting $\tau_{H_2O} = 1$, invoking the ideal gas law and hydrostatic balance to write pressure as

$$p = p_{ref}(T/T_{ref})^{g/\Gamma R_d}, \tag{A2}$$

where T_{ref} is the temperature at p_{ref}, and solving for T_{em} as per Equation 3 results in the emission temperatures as a function of absorption coefficients:

$$T_{em}(\kappa_{H_2O}) = \frac{T^*}{W\left(\frac{T^*}{T_{ref}}(D \cdot \mathrm{RH} \cdot M_v \cdot \kappa_{H_2O})^{R_d\Gamma/g}\right)}, \tag{A3}$$

where $T^* \equiv LR_d\Gamma/(gR_v) \approx 960$ K is a characteristic temperature for water vapor (see Jeevanjee & Fueglistaler, 2020b for details), W is the Lambert-W function which inverts the function $y = x\exp(x)$, $D = 1.5$ arises from the two stream approximation in radiative transfer theory, $\Gamma = 7$ K km^{-1} is the globally-averaged lapse rate of the troposphere in the GCM used later on (Figure S1b in Supporting Information S1), $M_v \approx 6 \cdot 10^9$ kg m^{-2} is a characteristic column water vapor mass, T_{ref} is the atmospheric temperature at $p_{ref} = 500hPa$, RH is column RH, and all other symbols have their usual meaning (see also Table S1 in Supporting Information S1 for values and meanings of the variables and constants).

Conflict of Interest

The authors declare no conflicts of interest relevant to this study.

Data Availability Statement

The Isca simulation data used for studying the tropopause in this study are made available in `mckimb/tropopause-v0.0.0`, a Zenodo repository located at https://doi.org/10.5281/zenodo.13150073 (McKim, 2024). This code includes the run scripts to produce simulations, as well as data analysis and plotting scripts used to create the figures in the manuscript.

Acknowledgments
BAM was funded by the University of Exeter. GKV also acknowledges support from NERC under the CIRCULATES grant NE/T006285/1. For the purpose of open access, the authors have applied a Creative Commons Attribution (CC BY) license to any Author Accepted Manuscript version arising from this submission.

References

Birner, T. (2010). Residual circulation and tropopause structure. *Journal of the Atmospheric Sciences*, *67*(8), 2582–2600. https://doi.org/10.1175/2010JAS3287.1

Byrne, M. P., & O'Gorman, P. A. (2013). Land–ocean warming contrast over a wide range of climates: Convective quasi-equilibrium theory and idealized simulations. *Journal of Climate*, *26*(12), 4000–4016. https://doi.org/10.1175/JCLI-D-12-00262.1

Clough, S. A., Iacono, M. J., & Moncet, J.-L. (1992). Line-by-line calculations of atmospheric fluxes and cooling rates: Application to water vapor. *Journal of Geophysical Research*, *97*(D14), 15761–15785. https://doi.org/10.1029/92JD01419

Dacie, S., Kluft, L., Schmidt, H., Stevens, B., Buehler, S. A., Nowack, P. J., et al. (2019). A 1d rce study of factors affecting the tropical tropopause layer and surface climate. *Journal of Climate*, *32*(20), 6769–6782. https://doi.org/10.1175/JCLI-D-18-0778.1

Dessler, A. E., Schoeberl, M. R., Wang, T., Davis, S. M., & Rosenlof, K. H. (2013). Stratospheric water vapor feedback. *Proceedings of the National Academy of Sciences*, *110*(45), 18087–18091. https://doi.org/10.1073/pnas.1310344110

Emanuel, K. (2006). Hurricanes: Tempests in a greenhouse. *Physics Today*, *59*(8), 74–75. https://doi.org/10.1063/1.2349743

Emanuel, K., Solomon, S., Folini, D., Davis, S., & Cagnazzo, C. (2013). Influence of tropical tropopause layer cooling on atlantic hurricane activity. *Journal of Climate*, *26*(7), 2288–2301. https://doi.org/10.1175/JCLI-D-12-00242.1

Feng, J., Paynter, D., & Menzel, R. (2023). How a stable greenhouse effect on earth is maintained under global warming. *Journal of Geophysical Research: Atmospheres*, *128*(9), e2022JD038124. https://doi.org/10.1029/2022JD038124

Fildier, B., Muller, C., Pincus, R., & Fueglistaler, S. (2023). How moisture shapes low-level radiative cooling in subsidence regimes. *AGU Advances*, *4*(3), e2023AV000880. https://doi.org/10.1029/2023AV000880

Frierson, D. M. W. (2007). The dynamics of idealized convection schemes and their effect on the zonally averaged tropical circulation. *Journal of the Atmospheric Sciences*, *64*(6), 1959–1976. https://doi.org/10.1175/JAS3935.1

Frierson, D. M. W., Held, I. M., & Zurita-Gotor, P. (2006). A gray-radiation aquaplanet moist gcm. part i: Static stability and eddy scale. *Journal of the Atmospheric Sciences*, *63*(10), 2548–2566. https://doi.org/10.1175/JAS3753.1

Fu, Q. (2006). 4 - Radiative transfer. In J. M. Wallace & P. V. Hobbs (Eds.), *Atmospheric science* (Second Edition ed., pp. 113–152). Academic Press. https://doi.org/10.1016/B978-0-12-732951-2.50009-0

Fueglistaler, S., Dessler, A. E., Dunkerton, T. J., Folkins, I., Fu, Q., & Mote, P. W. (2009). Tropical tropopause layer. *Reviews of Geophysics*, *47*(1), RG1004. https://doi.org/10.1029/2008RG000267

Gettelman, A., Forster, P. M. d. F., Fujiwara, M., Fu, Q., Vömel, H., Gohar, L. K., et al. (2004). Radiation balance of the tropical tropopause layer. *Journal of Geophysical Research*, *109*(D7), D07103. https://doi.org/10.1029/2003JD004190

Goody, R. M., & Yung, Y. L. (1989). *Atmospheric Radiation: Theoretical Basis*. Oxford University Press.

Gordon, I., Rothman, L., Hill, C., Kochanov, R., Tan, Y., Bernath, P., et al. (2017). The hitran2016 molecular spectroscopic database. *Journal of Quantitative Spectroscopy and Radiative Transfer*, *203*(HITRAN2016 Special Issue), 3–69. https://doi.org/10.1016/j.jqsrt.2017.06.038

Haqq-Misra, J., Lee, S., & Frierson, D. M. W. (2011). Tropopause structure and the role of eddies. *Journal of the Atmospheric Sciences*, *68*(12), 2930–2944. https://doi.org/10.1175/JAS-D-11-087.1

Harrop, B. E., & Hartmann, D. L. (2012). Testing the role of radiation in determining tropical cloud-top temperature. *Journal of Climate*, *25*(17), 5731–5747. https://doi.org/10.1175/JCLI-D-11-00445.1

Hartmann, D. L., & Larson, K. (2002). An important constraint on tropical cloud - Climate feedback. *Geophysical Research Letters*, *29*(20), 12-1–12-4. https://doi.org/10.1029/2002GL015835

He, H., Kramer, R. J., Soden, B. J., & Jeevanjee, N. (2023). State dependence of co2 forcing and its implications for climate sensitivity. *Science*, *382*(6674), 1051–1056. https://doi.org/10.1126/science.abq6872

Held, I. M. (1982). On the height of the tropopause and the static stability of the troposphere. *Journal of the Atmospheric Sciences*, *39*(2), 412–417. https://doi.org/10.1175/1520-0469(1982)039⟨0412:OTHOTT⟩2.0.CO;2

Held, I. M., & Soden, B. J. (2006). Robust responses of the hydrological cycle to global warming. *Journal of Climate*, *19*(21), 5686–5699. https://doi.org/10.1175/JCLI3990.1

Highwood, E. J., & Hoskins, B. J. (1998). The tropical tropopause. *Quarterly Journal of the Royal Meteorological Society*, *124*(549), 1579–1604. https://doi.org/10.1002/qj.49712454911

Hu, S., & Vallis, G. K. (2019). Meridional structure and future changes of tropopause height and temperature. *Quarterly Journal of the Royal Meteorological Society*, *145*(723), 2698–2717. https://doi.org/10.1002/qj.3587

Jeevanjee, N. (2023). Climate sensitivity from radiative-convective equilibrium: A chalkboard approacha). *American Journal of Physics*, *91*(9), 731–745. https://doi.org/10.1119/5.0135727

Jeevanjee, N., & Fueglistaler, S. (2020a). On the cooling-to-space approximation. *Journal of the Atmospheric Sciences*, *77*(2), 465–478. https://doi.org/10.1175/JAS-D-18-0352.1

Jeevanjee, N., & Fueglistaler, S. (2020b). Simple spectral models for atmospheric radiative cooling. *Journal of the Atmospheric Sciences*, *77*(2), 479–497. https://doi.org/10.1175/JAS-D-18-0347.1

Jeevanjee, N., Seeley, J. T., Paynter, D., & Fueglistaler, S. (2021). An analytical model for spatially varying clear-sky co2 forcing. *Journal of Climate*, *34*(23), 9463–9480. https://doi.org/10.1175/JCLI-D-19-0756.1

Kang, S. M., Frierson, D. M. W., & Held, I. M. (2009). The tropical response to extratropical thermal forcing in an idealized gcm: The importance of radiative feedbacks and convective parameterization. *Journal of the Atmospheric Sciences*, *66*(9), 2812–2827. https://doi.org/10.1175/2009JAS2924.1

Koll, D. B., & Cronin, T. W. (2018). Earth's outgoing longwave radiation linear due to h2o greenhouse effect. *Proceedings of the National Academy of Sciences*, *115*(41), 10293–10298. https://doi.org/10.1073/pnas.1809868115

Koll, D. D. B., Jeevanjee, N., & Lutsko, N. J. (2023). An analytic model for the clear-sky longwave feedback. *Journal of the Atmospheric Sciences*, *80*(8), 1923–1951. https://doi.org/10.1175/JAS-D-22-0178.1

Kuang, Z., & Hartmann, D. L. (2007). Testing the fixed anvil temperature hypothesis in a cloud-resolving model. *Journal of Climate*, *20*(10), 2051–2057. https://doi.org/10.1175/JCLI4124.1

Kubar, T. L., Hartmann, D. L., & Wood, R. (2007). Radiative and convective driving of tropical high clouds. *Journal of Climate*, *20*(22), 5510–5526. https://doi.org/10.1175/2007JCLI1628.1

Lin, P., Paynter, D., Ming, Y., & Ramaswamy, V. (2017). Changes of the tropical tropopause layer under global warming. *Journal of Climate*, *30*(4), 1245–1258. https://doi.org/10.1175/jcli-d-16-0457.1

Lorenz, D. J., & DeWeaver, E. T. (2007). Tropopause height and zonal wind response to global warming in the ipcc scenario integrations. *Journal of Geophysical Research*, *112*(D10), D10119. https://doi.org/10.1029/2006JD008087

Manabe, S., & Strickler, R. F. (1964). Thermal equilibrium of the atmosphere with a convective adjustment. *Journal of the Atmospheric Sciences*, *21*(4), 361–385. https://doi.org/10.1175/1520-0469(1964)021⟨0361:TEOTAW⟩2.0.CO;2

Match, A., & Gerber, E. P. (2022). Tropospheric expansion under global warming reduces tropical lower stratospheric ozone. *Geophysical Research Letters*, *49*(19), e2022GL099463. https://doi.org/10.1029/2022GL099463

McKim, B. (2024). mckimb/tropopause: Tropopause scripts and data for peer review [Dataset and software]. *Zenodo*(v0.0.0). https://doi.org/10.5281/zenodo.13150074

Meraner, K., Mauritsen, T., & Voigt, A. (2013). Robust increase in equilibrium climate sensitivity under global warming. *Geophysical Research Letters*, *40*(22), 5944–5948. https://doi.org/10.1002/2013GL058118

Mlawer, E. J., Taubman, S. J., Brown, P. D., Iacono, M. J., & Clough, S. A. (1997). Radiative transfer for inhomogeneous atmospheres: Rrtm, a validated correlated-k model for the longwave. *Journal of Geophysical Research*, *102*(D14), 16663–16682. https://doi.org/10.1029/97JD00237

Mote, P. W., Rosenlof, K. H., McIntyre, M. E., Carr, E. S., Gille, J. C., Holton, J. R., et al. (1996). An atmospheric tape recorder: The imprint of tropical tropopause temperatures on stratospheric water vapor. *Journal of Geophysical Research*, *101*(D2), 3989–4006. https://doi.org/10.1029/95JD03422

Nakajima, S., Hayashi, Y.-Y., & Abe, Y. (1992). A study on the "runaway greenhouse effect" with a one-dimensional radiative–convective equilibrium model. *Journal of the Atmospheric Sciences*, *49*(23), 2256–2266. https://doi.org/10.1175/1520-0469(1992)049⟨2256:ASOTGE⟩2.0.CO;2

Neale, R. B., & Hoskins, B. J. (2000). A standard test for agcms including their physical parametrizations: I: The proposal. *Atmospheric Science Letters*, *1*(2), 101–107. https://doi.org/10.1006/asle.2000.0022

O'Gorman, P. A. (2011). The effective static stability experienced by eddies in a moist atmosphere. *Journal of the Atmospheric Sciences*, *68*(1), 75–90. https://doi.org/10.1175/2010JAS3537.1

O'Gorman, P. A., & Schneider, T. (2008). The hydrological cycle over a wide range of climates simulated with an idealized GCM. *Journal of Climate*, *21*(15), 3815–3832. https://doi.org/10.1175/2007JCLI2065.1

Parmentier, V., & Guillot, T. (2014). A non-grey analytical model for irradiated atmospheres. I. Derivation. *Astronomy and Astrophysics*, *562*, 133. https://doi.org/10.1051/0004-6361/201322342

Petty, G. (2006). *A first course in atmospheric radiation*. Sundog Pub.

Phillips, N. A. (1956). The general circulation of the atmosphere: A numerical experiment. *Quarterly Journal of the Royal Meteorological Society*, *82*(352), 123–164. https://doi.org/10.1002/qj.49708235202

Pierrehumbert, R. T. (2010). *Principles of planetary climate*. Cambridge University Press. https://doi.org/10.1017/CBO9780511780783

Randel, W. J., & Jensen, E. J. (2013). Physical processes in the tropical tropopause layer and their roles in a changing climate. *Nature Geoscience*, *6*(3), 169–176. https://doi.org/10.1038/ngeo1733

Rauscher, E., & Menou, K. (2012). A general circulation model for gaseous exoplanets with double-gray radiative transfer. *The Astrophysical Journal*, *750*(2), 96. https://doi.org/10.1088/0004-637X/750/2/96

Robinson, T. D., & Catling, D. C. (2014). Common 0.1 bar tropopause in thick atmospheres set by pressure-dependent infrared transparency. *Nature Geoscience*, *7*(1), 12–15. https://doi.org/10.1038/ngeo2020

Romps, D. M. (2016). Clausius–clapeyron scaling of cape from analytical solutions to rce. *Journal of the Atmospheric Sciences*, *73*(9), 3719–3737. https://doi.org/10.1175/JAS-D-15-0327.1

Romps, D. M., Seeley, J. T., & Edman, J. P. (2022). Why the forcing from carbon dioxide scales as the logarithm of its concentration. *Journal of Climate*, *35*(13), 4027–4047. https://doi.org/10.1175/jcli-d-21-0275.1

Santer, B. D., Sausen, R., Wigley, T. M. L., Boyle, J. S., AchutaRao, K., Doutriaux, C., et al. (2003). Behavior of tropopause height and atmospheric temperature in models, reanalyses, and observations: Decadal changes. *Journal of Geophysical Research*, *108*(D1), ACL1-1–ACL1-22. https://doi.org/10.1029/2002JD002258

Schneider, T. (2004). The tropopause and the thermal stratification in the extratropics of a dry atmosphere. *Journal of the Atmospheric Sciences*, *61*(12), 1317–1340. https://doi.org/10.1175/1520-0469(2004)061⟨1317:TTATTS⟩2.0.CO;2

Schneider, T. (2008). Chapter 3 the thermal stratification of the extratropical troposphere. In *The global circulation of the atmosphere* (pp. 47–77). Princeton University Press. https://doi.org/10.1515/9780691236919-005

Schneider, T., & O'Gorman, P. A. (2008). Moist convection and the thermal stratification of the extratropical troposphere. *Journal of the Atmospheric Sciences*, *65*(11), 3571–3583. https://doi.org/10.1175/2008JAS2652.1

Schneider, T., O'Gorman, P. A., & Levine, X. J. (2010). Water vapor and the dynamics of climate changes. *Reviews of Geophysics*, *48*(3), RG3001. https://doi.org/10.1029/2009RG000302

Seeley, J. T., Jeevanjee, N., & Romps, D. M. (2019). Fat or fitt: Are anvil clouds or the tropopause temperature invariant? *Geophysical Research Letters*, *46*(3), 1842–1850. https://doi.org/10.1029/2018GL080096

Seidel, S. D., & Yang, D. (2022). Temperatures of anvil clouds and radiative tropopause in a wide array of cloud-resolving simulations. *Journal of Climate*, *35*(24), 8065–8078. https://doi.org/10.1175/JCLI-D-21-0962.1

Solomon, S., Rosenlof, K. H., Portmann, R. W., Daniel, J. S., Davis, S. M., Sanford, T. J., & Plattner, G.-K. (2010). Contributions of stratospheric water vapor to decadal changes in the rate of global warming. *Science*, *327*(5970), 1219–1223. https://doi.org/10.1126/science.1182488

Spaulding-Astudillo, F. E., & Mitchell, J. L. (2023). Effects of varying saturation vapor pressure on climate, clouds, and convection. *Journal of the Atmospheric Sciences*, *80*(5), 1247–1266. https://doi.org/10.1175/JAS-D-22-0063.1

Spaulding-Astudillo, F. E., & Mitchell, J. L. (2025). Clear-sky convergence, water vapor spectroscopy, and the origin of tropical congestus clouds. *AGU Advances*, *6*, e2024AV001300. https://doi.org/10.1029/2024AV001300

Stevens, B., & Bony, S. (2013). Water in the atmosphere. *Physics Today*, *66*(6), 29–34. https://doi.org/10.1063/PT.3.2009

Stevens, B., & Kluft, L. (2023). *A colorful look at climate sensitivity* (Vol. 2023, pp. 1–24). EGUsphere. https://doi.org/10.5194/egusphere-2022-1460

Stone, P. H., & Carlson, J. H. (1979). Atmospheric lapse rate regimes and their parameterization. *Journal of the Atmospheric Sciences*, *36*(3), 415–423. https://doi.org/10.1175/1520-0469(1979)036⟨0415:ALRRAT⟩2.0.CO;2

Tan, Z., Lachmy, O., & Shaw, T. A. (2019). The sensitivity of the jet stream response to climate change to radiative assumptions. *Journal of Advances in Modeling Earth Systems*, *11*(4), 934–956. https://doi.org/10.1029/2018MS001492

Thompson, D. W. J., Bony, S., & Li, Y. (2017). Thermodynamic constraint on the depth of the global tropospheric circulation. *Proceedings of the National Academy of Sciences*, *114*(31), 8181–8186. https://doi.org/10.1073/pnas.1620493114

Thompson, D. W. J., Ceppi, P., & Li, Y. (2019). A robust constraint on the temperature and height of the extratropical tropopause. *Journal of Climate*, *32*(2), 273–287. https://doi.org/10.1175/JCLI-D-18-0339.1

Thuburn, J., & Craig, G. C. (2000). Stratospheric influence on tropopause height: The radiative constraint. *Journal of the Atmospheric Sciences*, *57*(1), 17–28. https://doi.org/10.1175/1520-0469(2000)057⟨0017:SIOTHT⟩2.0.CO;2

Thuburn, J., & Craig, G. C. (2002). On the temperature structure of the tropical substratosphere. *Journal of Geophysical Research*, *107*(D2), ACL10-1–ACL10-10. https://doi.org/10.1029/2001JD000448

Troen, I. B., & Mahrt, L. (1986). A simple model of the atmospheric boundary layer; sensitivity to surface evaporation. *Boundary-Layer Meteorology*, *37*(1–2), 129–148. https://doi.org/10.1007/BF00122760

Vallis, G. K. (2017). *Atmospheric and oceanic fluid dynamics: Fundamentals and large-scale circulation* (2nd ed.). Cambridge University Press. https://doi.org/10.1017/9781107588417

Vallis, G. K. (2020). The trouble with water: Condensation, circulation and climate. *The European Physical Journal Plus*, *135*(6), 478. https://doi.org/10.1140/epjp/s13360-020-00493-7

Vallis, G. K., Colyer, G., Geen, R., Gerber, E., Jucker, M., Maher, P., et al. (2018). Isca, v1.0: A framework for the global modelling of the atmospheres of earth and other planets at varying levels of complexity. *Geoscientific Model Development*, *11*(3), 843–859. https://doi.org/10.5194/gmd-11-843-2018

Vallis, G. K., Zurita-Gotor, P., Cairns, C., & Kidston, J. (2015). Response of the large-scale structure of the atmosphere to global warming. *Quarterly Journal of the Royal Meteorological Society*, *141*(690), 1479–1501. https://doi.org/10.1002/qj.2456

WMO. (1957). A three-dimensional science: Second session of the commission for aerology. *WMO bull*, *4*(2), 134–138.

Zelinka, M. D., & Hartmann, D. L. (2010). Why is longwave cloud feedback positive? *Journal of Geophysical Research*, *115*(D16), D16117. https://doi.org/10.1029/2010JD013817

Zurita-Gotor, P., & Vallis, G. K. (2011). Dynamics of midlatitude tropopause height in an idealized model. *Journal of the Atmospheric Sciences*, *68*(4), 823–838. https://doi.org/10.1175/2010JAS3631.1